Journal of
*Manufacturing and Materials Processing*

MDPI

*Article*

# In Vitro Characterization of 3D-Printed PLA/CPO Oxygen Releasing Scaffolds: Mechanical and Biological Properties for Bone Tissue Engineering

**Abdullah Mohammed [1,2], Alice Tirnoveanu [3], William Richard Webb [3], Ammar A. Melaibari [2,4], Adnan Memić [2], Mohammad Aslam [5], Amr Elshaer [6], Hany Hassanin [7,*] and Khamis Essa [1,*]**

1 School of Engineering, University of Birmingham, Birmingham B15 2TT, UK; axm1777@student.bham.ac.uk
2 Centre of Nanotechnology, King Abdulaziz University, Jeddah P.O. Box 80204, Saudi Arabia; aamelaibari@kau.edu.sa (A.A.M.); amemic@kau.edu.sa (A.M.)
3 Institute of Medical Sciences, Faculty of Medicine, Health and Social Care, Canterbury Christ Church University, Canterbury CT1 1QU, UK; alice.tirnoveanu@canterbury.ac.uk (A.T.); w.r.webb1@icloud.com (W.R.W.)
4 Mechanical Engineering Department, Faculty of Engineering, King Abdulaziz University (KAU), Jeddah P.O. Box 80204, Saudi Arabia
5 Centre of Excellence in Environmental Studies, King Abdulaziz University, Jeddah P.O. Box 80204, Saudi Arabia; magmuhammad21@kau.edu.sa
6 Drug Discovery, Delivery and Patient Care (DDDPC), School of Life Sciences, Pharmacy and Chemistry, Kingston University London, Kingston Upon Thames KT1 2EE, UK; a.elshaer@kingston.ac.uk
7 School of Engineering, Canterbury Christ Church University, Canterbury CT1 1QU, UK
* Correspondence: hany.hassanin@canterbury.ac.uk (H.H.); k.e.a.essa@bham.ac.uk (K.E.)

**Abstract:** The addition of oxygen-releasing biomaterials into 3D-printed scaffolds presents a novel approach to enhancing bone scaffolds, yet no in vitro studies have demonstrated the effect of oxygen-generating filaments on scaffold biological and mechanical properties. This study introduces a polylactic acid (PLA)/calcium peroxide (CPO) composite filament, designed for oxygen release, which is a key factor for early-stage bone regeneration. The PLA/CPO composite filament was fabricated via wet-mixing, solvent evaporation, and hot-melt extrusion, followed by fused deposition modeling (FDM) with optimized parameters to achieve high structural fidelity (25% porosity, 0.60mm pore size). In vitro characterization, including mechanical, morphological, and biological assessments, demonstrated that, post-cell culturing, mechanical strength improved, which indicates improved scaffold resilience. The scaffold exhibited gradual oxygen release over a 3-day period, and gene expression analysis confirmed notable upregulation of osteogenic markers RUNX2, SPP1, and SP7 in vitamin D-supplemented conditions. The mechanical strength improved from approximately 2.8 MPa in the control group to 5.0 MPa in scaffolds cultured with osteogenic media. This study provides the first in vitro evidence that oxygen-releasing 3D-printed filaments can improve both mechanical properties and biological response in scaffolds, demonstrating the functional integration of sustained oxygen delivery, enhanced mechanical properties, and increased osteogenic activity in a single 3D-printed scaffold.

**Keywords:** 3D printing; oxygen-generating scaffolds; PLA/CPO composite; bone tissue regeneration; fused deposition modeling (FDM)

check for updates

Academic Editor: Steven Y. Liang

Received: 28 March 2025
Revised: 24 April 2025
Accepted: 27 April 2025
Published: 2 May 2025

**Citation:** Mohammed, A.; Tirnoveanu, A.; Webb, W.R.; Melaibari, A.A.; Memić, A.; Aslam, M.; Elshaer, A.; Hassanin, H.; Essa, K. In Vitro Characterization of 3D-Printed PLA/CPO Oxygen Releasing Scaffolds: Mechanical and Biological Properties for Bone Tissue Engineering. *J. Manuf. Mater. Process.* **2025**, *9*, 149. https://doi.org/10.3390/jmmp9050149

**Copyright:** © 2025 by the authors. Licensee MDPI, Basel, Switzerland. This article is an open access article distributed under the terms and conditions of the Creative Commons Attribution (CC BY) license (https://creativecommons.org/licenses/by/4.0/).

## 1. Introduction

The rising need for organ transplants and tissues has led to a severe shortage of available donors, creating a significant gap between supply and demand. This shortage

represents a major biomedical challenge, with over 106,000 individuals in the United States currently waiting for a transplant. According to data from March 2022, this shortage has tragic consequences, as 17 people die each day while waiting for a transplant due to delays in receiving the necessary organs [1]. Bones are among the most highly sought-after tissues for transplantation in the United States, and finding a donor match is a significant challenge for bone graft procedures [2]. Autografts, which utilize tissue from the patient's own body, are widely considered the best option for bone fracture repair and regeneration. This method promotes healing by using the patient's natural tissue, minimizing the risk of rejection. However, autografts are not always practical, particularly in cases where the bone defect is too large to repair with the available tissue or when highly precise shaping is required, as in complex facial bone surgeries. In such situations, alternative solutions must be explored to achieve successful outcomes [3]. Tissue engineering has become a viable alternative to bone grafting for bone regeneration. This method involves the creation of a bone scaffold that includes growth factors, stem cells, and biocompatible and biodegradable materials, which can aid in bone fracture healing and enhance the incorporation of the graft [4,5]. The scaffolds are specifically designed to provide essential structural support while promoting tissue regeneration. By mimicking the natural extracellular matrix, they create an environment that encourages cell growth and repair, ultimately assisting the tissue in recovering its functional capabilities [6–8].

Recently, the application of 3D printing technologies for producing bone scaffolds has attracted significant interest. This approach allows for the creation of scaffolds with specific external designs and porous internal structures, enabling the development of scaffolds with customized functionality [9,10]. Among the various 3D printing methods, fused deposition modeling (FDM) is frequently employed in tissue engineering due to its affordability, accessibility, and ease of use [11]. Moreover, FDM achieves a printing accuracy of up to $+/-0.5$ mm and can utilize a wide range of biocompatible and biodegradable polymeric materials suitable for tissue engineering [11,12].

Tissue engineering makes use of a variety of materials to repair bone, tendon, and skin. Among these, polycaprolactone (PCL), polylactic acid (PLA), and polyglycolide or poly-glycolic acid (PGA) are particularly useful due to their favorable mechanical and biochemical properties [13,14]. PLA is a material recognized for its beneficial physical and mechanical properties, alongside its biocompatibility and biodegradability. These attributes are significantly influenced by factors such as its molecular weight. Higher molecular weights generally enhance strength and durability [15]. Together, these factors determine how well PLA performs in various applications, especially in medical and tissue engineering contexts [16]. These properties make PLA an excellent candidate for a wide variety of industrial applications, particularly in the development of medical devices. Additionally, PLA is compatible with FDM 3D printers and has been approved by the US Food and Drug Administration (FDA) for several biomedical uses [17]. However, while tissue engineering has shown promising results in laboratory settings, its clinical application has been largely limited to treating small tissue defects, typically measuring just a few millimetres. This limitation stems from the difficulty in achieving adequate vascularization, which is crucial for supplying the necessary oxygen to support tissue survival and growth. Without sufficient blood vessel formation, larger tissue constructs struggle to receive the oxygen and nutrients they need, hindering their effectiveness in clinical settings [18,19]. The insufficient oxygen levels in engineered tissues are a significant barrier to bone regeneration and the overall effectiveness of scaffolds. This shortage restricts the growth of cells that attach to the scaffold, which is essential for successful tissue development [20].

Researchers have designed scaffolds that release oxygen by utilizing various solid peroxide particles, such as magnesium peroxide, calcium peroxide, and sodium percar-

bonate. The usual process involves the disintegration of these particles in water, resulting in the release of oxygen through hydrolysis, as displayed in Equations (1) and (2) [7,21]. Calcium peroxide (CPO) is frequently selected as an oxygen-releasing agent because it is both economical and widely available in the market, making it a practical choice compared to other materials [22–24].

$$CaO_2 + 2H_2O \rightarrow Ca(OH)_2 + H_2O_2 \quad (1)$$

$$2H_2O_2 \rightarrow O_2 + 2H_2O \quad (2)$$

Studies suggest that the fabrication of bone scaffolds incorporating 3D-printed oxygenation filaments can significantly enhance bone tissue regeneration and healing. The incorporation of an oxygen source within the scaffold has been found to promote vascularization and enhance the scaffold's efficacy [19]. The aim of this study is to investigate the in vitro performance of a newly developed oxygen-releasing PLA/CPO scaffold fabricated using FDM. This work is the first to assess the combined effects of sustained oxygen release, post-culture mechanical behavior, and osteogenic gene expression in bone stem cells.

## 2. Materials and Methods

### *2.1. Materials*

PLA filament with a diameter of 1.75 mm was purchased from the Shenzhen eSUN Industrial Co., Ltd. (Shenzhen, China). For the oxygen-releasing component, calcium peroxide (CPO) was obtained from Sigma-Aldrich (St. Louis, MO, USA); it has a particle size of 200 mesh and a purity of 75%. Additionally, catalase, derived from bovine serum with an activity level of 5000 units/mg, was also purchased from Sigma-Aldrich. Dichloromethane (DCM), a solvent used in various applications, was acquired from the same supplier, along with deionized water for use in the experiments.

### *2.2. PLA/CPO Filament*

PLA filaments (20 g) were first cut into small pieces and dissolved in 100 mL of DCM at room temperature for 30 min, using a magnetic stirrer set at 700 rpm. Once the PLA was fully dissolved, CPO powder was added to the PLA and the mixture was vigorously stirred for an additional 90 min to ensure thorough incorporation. The resulting homogeneous solution was then poured into a large plate and allowed to dry for 24 h. After drying, the composites were cut into smaller pieces suitable for loading into the hot melt extruder. A custom single-screw extruder with a nozzle diameter of 2 mm was employed to extrude the composite materials at a nozzle temperature of 140 °C and an extrusion speed of 2.5 cm/s. Figure 1 shows the schematic diagram of the process and the extruded filament under the microscope. The prepared PLA-CPO filaments were immersed in a phosphate-buffered saline (PBS) solution (pH 7.4), which mimics the pH and osmolarity of human fluids. Additionally, 10 mg of catalase was also added into the solution to catalyze the decomposition of hydrogen peroxide ($H_2O_2$) into water and oxygen, ensuring accurate detection of the oxygen-releasing capability of the material. Oxygen levels were measured in triplicate using an oxygen sensor to track the oxygen release on daily use.

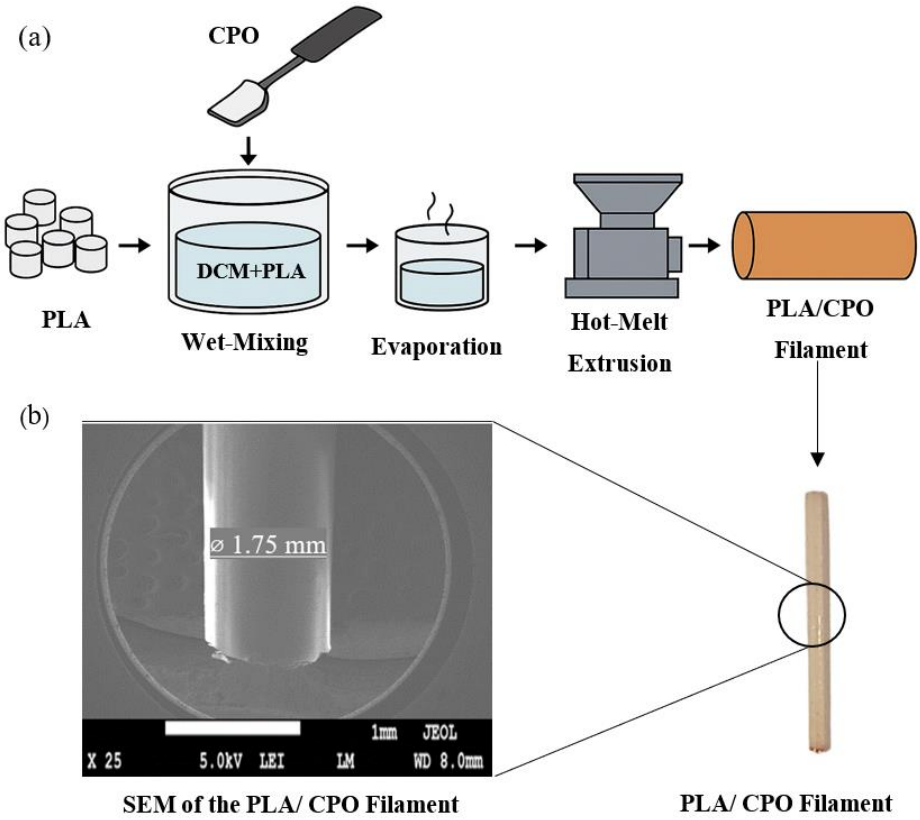



**Figure 1.** (**a**) Schematic diagram of the PLA-CPO composite filament process (**b**) the extruded filament under SEM.

### *2.3. 3D Printing of Bone Scaffolds*

A commercial Fused Deposition Modeling (FDM) 3D printer, specifically the Creality Ender 3 Pro, manufactured by the Shenzhen Creality 3D Technology Co., Ltd. in China, was utilized to fabricate the bone scaffolds under a range of parameters outlined in Table 1. The scaffolds were designed in a square shape, measuring 8 × 8 mm in both length and width, with a height of 1.5 mm. Each scaffold was engineered to have a porosity of 25%, featuring pores with a size of 0.60 mm. This design was intended to optimize the scaffolds for tissue regeneration by providing adequate support and permeability for cell growth.

**Table 1.** 3D printer parameters used to print PLA scaffolds.

| Sample No. | Printing Temperature (°C) | Building Platform Temperature (°C) | Printing Speed (mm/s) |
|---|---|---|---|
| 1 | 200 | 70 | 25 |
| 2 | 200 | 70 | 50 |
| 3 | 200 | 70 | 75 |

### *2.4. Characterizations*

#### 2.4.1. Morphological Analysis

The scaffolds were designed in a square shape, measuring 8 × 8 mm in both length and width, with a height of 1.5 mm. Each scaffold was engineered to have a porosity of 25%, featuring pores with a size of 0.60 mm. This design was intended to optimize the scaffolds for tissue regeneration by providing adequate support and permeability for cell growth. The micrograph images were used for morphological analysis using ImageJ 1.53f51, an open-source image analysis software developed by the National Institutes of Health

(NIH) in the USA. The contact angle was measured on printed scaffold samples using a KRÜSS DSA30E drop shape analyzer (Germany). The sessile drop method was employed with 10 μL deionized water droplets, dispensed at a rate of 2 μL/s. Measurements were performed at room temperature and averaged over three replicates per sample. The scaffold morphology was examined using a JEOL JSM-6010LA scanning electron microscope. Prior to imaging, samples were sputter-coated with a 5 nm gold layer using a Quorum Q150R ES sputter coater to improve surface conductivity. Digital images of the drops were analyzed by computer software (DSA4, version 2.1). The water droplets were placed on relatively flat scaffold regions. Given the porous nature of the scaffold, minor liquid bridging across interconnected pores was possible; however, multiple measurements were performed across different areas of the scaffold to mitigate this effect. The final contact angle values were averaged to ensure repeatability and accuracy. The data analysis focused on comparing contact angle variations at different printing speeds, correlating surface topology changes with material deposition behavior during printing.

#### 2.4.2. Osteogenic Differentiation In Vitro

Cell Culture:

Human mesenchymal stem cells (Lonza) were cultured in Dulbecco's Modified Eagle's Medium—GlutaMax, a nutrient-rich medium designed to support cell growth. This medium was supplemented with 5% ($v/v$) human platelet-rich plasma (PRP), which provides essential growth factors, as well as 1% ($v/v$) non-essential amino acids to promote cellular health and function. Additionally, 1% ($v/v$) penicillin-streptomycin-amphotericin was included to prevent bacterial and fungal contamination. The cells were maintained in this enriched environment for 2 weeks, allowing them to expand and prepare for subsequent seeding in experimental applications.

Post-expansion, the PLA rods were sterilized for 24 hrs in 100% ethanol and 1 hr post-sterilization the PLA rods were pretreated by soaking in PBS containing 10ng/mL fibronectin at 37 °C. After 1 hour, the rods were washed twice with sterile PBS, and then $4 \times 10^5$ cells were seeded onto each rod. The rods were then placed in a ST180 PLUS CO2 incubator (Benchmark Scientific, Darmstadt, Germany) for 20 min to facilitate cell attachment. After this incubation, the rods were submerged in KOSR media for 24 h. This media was formulated with Dulbecco's Modified Eagle's Medium—GlutaMax, enhanced by 10% ($v/v$) KnockOut™ Serum Replacement, along with 1% ($v/v$) non-essential amino acids and 1% ($v/v$) penicillin-streptomycin-amphotericin, ensuring an optimal environment for the cells to flourish. After 24 hrs, the rods were separated into two groups: Control group (KOSR without vitamin D), and experimental differentiation group (where the media was supplemented with vitamin D, Beta-glysophosphate, and ascorbic-2-phosphate).

In the negative control plate, the medium did not contain vitamin D. The media were changed twice weekly for both the control and differentiation group over 21 days. PLA-only scaffolds were not included as a control group. The experimental aim was to evaluate osteogenic responses of the PLA/CPO scaffold under different biological stimulation conditions. Each group was tested in triplicate ($n$ = 3), and the results were presented descriptively without statistical testing, reflecting the exploratory nature of the study.

RNA Extraction:

The rods were then placed in a ST180 PLUS $CO_2$ incubator (Benchmark Scientific, Darmstadt, Germany) for 20 min to facilitate cell attachment. After this incubation, the rods were submerged in KOSR media for 24 h. This media was formulated with Dulbecco's Modified Eagle's Medium—GlutaMax, enhanced by 10% ($v/v$) KnockOut™ Serum

Replacement, along with 1% (*v*/*v*) non-essential amino acids and 1% (*v*/*v*) penicillin-streptomycin-amphotericin, ensuring an optimal environment for the cells to flourish.

RNA Quantification:

The extracted RNA was quantified by absorbance reading at a 260/280 nm ration with Tecan i-200-Pro. The measurements were performed in triplicate. The mean concentration value per sample was used for further calculation in the qRT-PCR set-up.

Quantitative Real-Time Reverse Transcriptase Polymerase Chain Reaction (qRT-PCR)

For the analysis of gene expression related to Glyceraldehyde 3-phosphate dehydrogenase (GAPDH), Runt-related transcription factor 2 (RUNX2), and Collagen type I alpha 1 chain (COL1A1), Secreted Phosphoprotein 1 (SPP1), and Sp7 transcription factor (SP7), the Qiagen QuantiNova SYBR Green RT-PCR kit was used, according to the supplier's guidelines.

Customized primer sets for GAPDH, RUNX2, COL1A1, SPP1 and SP7 were previously designed and verified against the human cell line MG63 (Osteosarcoma) supplied by ATCC. All primer sequences were designed using human gene data from the Ensembl genome browser and the NCBI Gene database. The specificity of the alignments was evaluated using the NCBI Primer-BLAST tool. The RT-PCR reaction was organized as follows:

The fold change value was further analyzed against the GAPDH expression and vitamin D was normalized utilizing delta-delta Ct to calculate the fold change against the control sample KOSR.

#### 2.4.3. Mechanical and Microstructural Properties

To evaluate the mechanical properties of the filaments, a universal Instron 3367 testing machine (Norwood, MA, USA) equipped with a 30 kN load cell was employed. The testing involved tensile testing of the filament with diameters ranging from 1.75 mm to 1.95 mm and a length of 90 mm. The filaments were securely held in place using manual grips, and the machine's crosshead speed was maintained at a constant rate of 5 mm/min. Each experiment was conducted three times, and the average values were calculated for accuracy. The results are presented as the mean ± standard deviation (SD). An Ultima IV X-ray diffractometer (XRD) (Rigaku, Tokyo, Japan) equipped with Cu Kα radiation and referenced with the ICDD (PDF-2/release 2011 RDB) database, including DB card No. 01-071-4107, was used to analyze the extruded filaments. The measurements were conducted at a goniometer speed of 1.00 sec per step with a step size of 0.100°.

### *2.5. Statistical Analysis*

Each experiment was conducted in triplicate to ensure reliability, and the mean value was calculated from these trials. The results are presented as averages with the ± standard deviation (SD) to show variability. Data analysis and visualization were performed using Origin software (OriginPro 8.0, Origin Lab Inc., Northampton, MA, USA), which helped create clear graphical representations of the findings.

## 3. Results and Discussion

### *3.1. 3D Printing of Scaffolds*

During extrusion, filaments containing 6% CPO exhibited optimal extrudability, forming smooth and uniform filaments suitable for 3D printing. In contrast, higher CPO concentrations led to increased brittleness, compromising both the printability and structural integrity. Therefore, a CPO concentration of 6% was maintained across all experiments to ensure consistent material performance and reproducibility in the biological evaluations. The release of oxygen of the PLA/CPO filament is shown in Figure 2. The oxygen release

profile demonstrates a gradual increase in oxygen concentration over 3 days. It shows that the embedded CPO undergoes hydrolysis at a steady rate. While the oxygen release results cover a short period (days), bone tissue regeneration is a long process that takes weeks to months. However, the evidence of early oxygenation provided by the PLA/CPO can play a key role in angiogenesis and osteogenic differentiation, which are fundamental steps in bone healing. The early release ensures that cells survive and proliferate in the initial hypoxic environment, supporting early vascularization before nutrition and the blood supply establishes. Further studies are needed to optimize oxygen release duration to extend beyond 3 days and sustain oxygen delivery throughout the healing process [25].

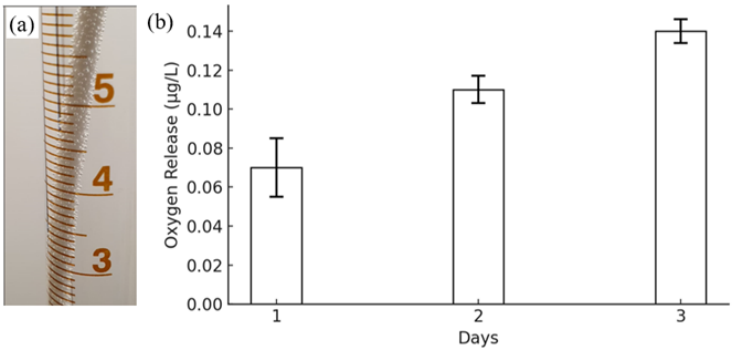



**Figure 2.** (**a**) Image of oxygen released during the degradation process shown as bubbles from the filaments (**b**) Oxygen release of the PLA/CPO filaments over a 3-day period.

Figure 3 presents optical images of the 3D-printed PLA/CPO scaffolds with both a side view and a top view of the scaffold structure. The figure demonstrates the pores and surface features of the printed scaffold sample. The distinct layers also highlight how the printing parameters, such as speed, contribute to the scaffold's vertical integrity. At lower speeds, scaffolds typically show uneven layer heights, but at higher speeds, as represented in Figure 3a, the layers appear smoother and more uniform, correlating with the findings on accuracy. The 3D printer parameters were mainly determined by two variables: temperature and speed of printing. While maintaining the temperature constant at ~200 °C, the printing speed was set to three different levels (Table 1). Figure 3b shows the pores are regularly spaced and exhibit a high degree of uniformity. This uniformity was more pronounced at higher printing speeds, such as 75 mm/s, where the accuracy reached 98.33%. The well-formed pores, critical for nutrient exchange and cell infiltration in tissue engineering, align with the structural requirements for bone scaffolds. At lower speeds, the pores tend to show overlap or deformation. The optical images serve as visual proof of the scaffold's dimensional accuracy and porosity. The pore interconnectivity and size suggest that the PLA/CPO composite scaffold is likely to facilitate effective cell proliferation and differentiation, matching the requirements outlined in the literature.

Moreover, Mota et al. noted that scaffolds with regular pore distribution support enhanced tissue integration, which can be inferred from the top view in Figure 3. The consistency of the pore shapes and the absence of irregularities further corroborate the improvements in accuracy and quality at higher printing speeds, reinforcing the conclusions drawn from previous sections of the analysis [26].

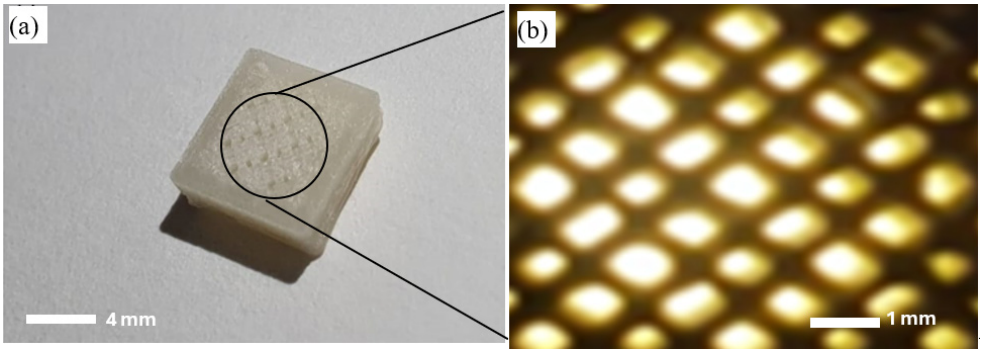



**Figure 3.** Optical images of the 3D printed scaffolds (**a**) side image and (**b**) top image with lighting source showing porosity.

The 3D printing of bone scaffolds using PLA/CPO composite material (Figure 3) was investigated to achieve the highest accuracy and quality. The 3D printer parameters were mainly determined by two variables: temperature and speed of printing. While maintaining the temperature constant at ~200 °C, the printing speed was set to three different levels (Table 1). The dimensional accuracy of the printed scaffolds at different speeds was determined based on the number of pores fabricated without overlapping or defacing the original design.

Figure 4 presents a detailed analysis of the accuracy, quality, and surface characteristics of the 3D-printed PLA/CPO scaffolds at various printing speeds (25 mm/s, 50 mm/s, and 75 mm/s). This figure provides quantitative data and visual insights into how the printing speed influences key aspects of scaffold formation, including the dimensional accuracy, slope angles, layer line width, and rough surface. The graph in Figure 4a shows a linear relationship between accuracy and printing speed. The graph in Figure 4a demonstrates a clear linear relationship between the printing speed and dimensional accuracy of the scaffolds. As the speed increases from 25 mm/s to 75 mm/s, the accuracy improves significantly, with the highest accuracy of 98.33% achieved at 75 mm/s. At 25 mm/s, the accuracy is drastically lower, around 48%, which indicates that at lower speeds, the printed pores are either deformed or overlap due to excessive material deposition or nozzle movement inconsistencies. At 50 mm/s, the accuracy improves but remains suboptimal compared to the highest speed. The optimal accuracy at 75 mm/s indicates that a faster printing speed allows for more precise material deposition without compromising the pore structure.

Figure 4b highlights how the printing speed affects the layer line width of the printed scaffolds. At lower speeds of 25 mm/s, the layer line width is inconsistent and irregular, contributing to a rougher surface. However, at 75 mm/s, the width becomes much more uniform, with a measured width of 0.40 mm. The slope angle, which indicates the angle between the layers, is much steeper at lower speeds (about 18° at 25 mm/s). This steeper angle leads to less even material distribution. As the speed increases, the slope angle decreases to 11.5° at 75 mm/s, resulting in a smoother and more stable surface structure, crucial for scaffold integrity. Typically, smoother layer transitions and reduced slope angles at higher speeds improve scaffold functionality by enhancing structural homogeneity.

Figure 4c compares the water contact angles of scaffolds printed at different speeds, which reflects surface morphology. The contact angle increases with speed, showing 96.5° at 25 mm/s, 97° at 50 mm/s, and 103° at 75 mm/s. A higher contact angle indicates a smoother and more hydrophobic surface. At higher speeds, the smoother surface reduces the roughness, thus increasing the contact angle. This suggests improved surface quality, as rougher surfaces typically lead to lower contact.

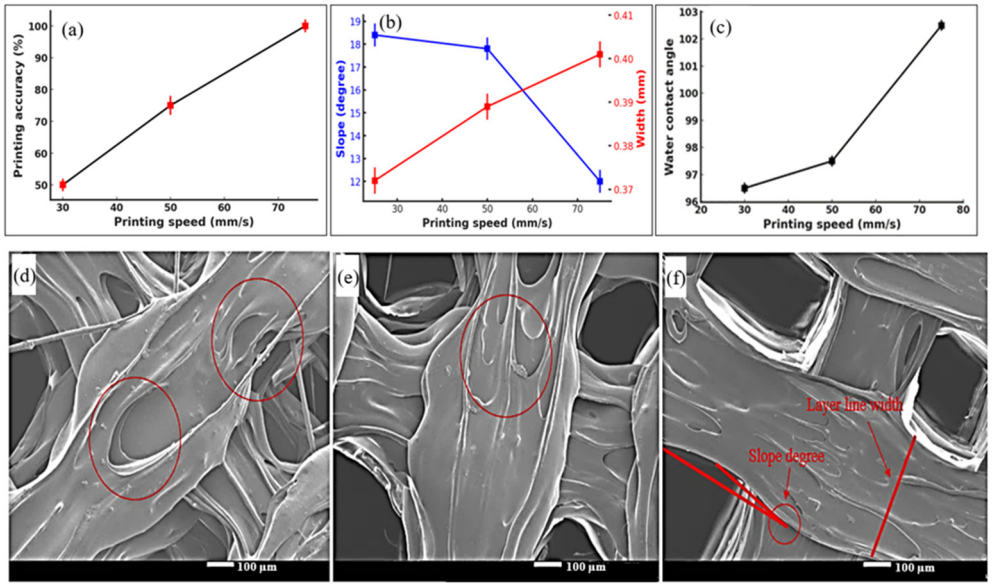



**Figure 4.** Evaluation of 3D printing accuracy and quality, (**a**) accuracy percentages of printed scaffolds at different printing speeds, (**b**) slope degree and width of scaffolds layer line at different printing speeds, and (**c**) water contact angles of printed scaffolds surface at different printing speeds. SEM images of printed scaffolds layer at different printing speeds of: (**d**) 25 mm/s, (**e**) 50 mm/s, and (**f**) 75 mm/s, ($n$ = 3).

The SEM image in Figure 4d shows significant surface roughness and irregular layer formation. The material appears uneven, with visible ridges and cavities. This highlights the negative effect of low-speed printing, where excess material accumulates, creating a rough, uneven surface. While the surface becomes smoother than at 25 mm/s, Figure 4e, some irregularities remain, suggesting moderate improvements in layer deposition and surface roughness. At the highest speed, Figure 4f, the SEM image displays a much smoother, more even surface. The layers are well aligned, with minimal defects or ridges. This significant improvement in surface morphology at high speed confirms the trend observed in both the accuracy and water contact angle measurements. Generally, a smoother surface will have a higher contact angle, while a rougher surface will have a lower contact angle [27]. Furthermore, it is clear from Figure 4d–f that the surface roughness becomes smoother and more symmetrical as the printing speed is increased. It was reported by Wangwang while printing an object with 100% infill that printing at high speed can cause cavities and delamination at the interface between different layers [28], which is opposite to our findings. It can be argued that our case is different from what has been reported in the literature because our composite material has a higher viscosity compared to pure PLA, making it more viscous due to the embedded CPO particles within the PLA matrix [29]. Hence, printing parameters for high accuracy and quality can vary depending on the materials used, as they are highly influenced by the materials' properties. As a result with the PLA/CPO composite, a higher extruding speed is required to achieve the desired accuracy and quality.

### *3.2. Gene Expression*

Skeleton can be either formed by intramembranous ossification or endochondral ossification. Mesenchymal cells differentiate directly into osteoblasts, which lead to the formation of intramembranous bones [30]. On the other hand, the replacement of the cartilaginous structure by bone will form endochondral bones. Around 90% of bone is made of type 1 collagen [31]. The latter is a triple helix structure made of 2 type 1 collagen strand (Col1a1) and on Col1a2 strand [32]. Furthermore, Col1a1 and Col1a2, as well as various transcription

factors are involved in bone development and maintenance. One important transcription factor is RUNX2, which is essential for osteoblast differentiation and bone formation [33]. Another significant factor is phosphoprotein 1 (Spp1), also known as osteopenia, produced by osteoblasts. Spp1 plays a crucial role in regulating bone mineralization and remodeling processes [34]. SP7, another transcription factor, is involved in osteoblast differentiation and mineralization [35]. In the present experimental configuration, the combination of scaffold composition and culture conditions led to an enhancement in the gene expression of Human Mesenchymal stem cells (hMSCs), cells associated with bone development in contrast to those grown in a monolayer. The upregulation of RUNX2 reflects the early-stage commitment of hMSCs to the osteoblast lineage. SP7, acting downstream of RUNX2, supports osteoblast maturation, while SPP1 (osteopontin) is a late marker involved in extracellular matrix organization and mineralization. The observed co-activation of these markers suggests progression through multiple stages of osteogenic differentiation.

In Figure 5, the gene expression results were normalized to the control filaments which were cultured in the absence of vitamin D. When Human Mesenchymal stem cells (hMSCs) were differentiated in the presence of vitamin D upregulation of the bone transcription factors essential for bone differentiation, (RUNX2, SPP1, and SP7) were observed. Conversely, a downregulation of COL1A1 was noted (Figure 5). Notably, a distinct increase was detected in the expression of RUNX2 genes in hMSC cells cultured, in contrast to the expression levels of COL1a1, SPP1, and SP7 genes, as well as the literature [36]. The downregulation of COL1A1 under vitamin D stimulation may reflect a biological shift from matrix production to mineralization, a phenomenon reported during later osteogenic stages. These results indicate that the oxygen-releasing scaffold, in combination with vitamin D, fosters an environment conducive to both early (RUNX2) and late (SPP1) osteogenic differentiation phases.

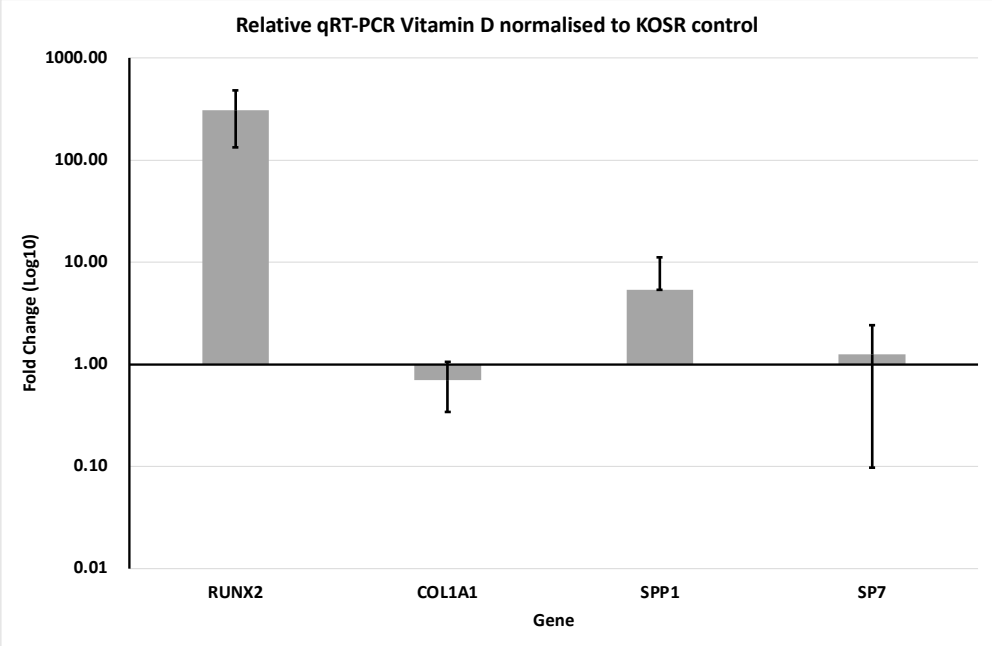



**Figure 5.** Delta-Delta Ct values for hMSCs differentiated in the presence of vitamin D ($n$ = 3).

### *3.3. Mechanical Properties*

The XRD in Figure 6a shows the microstructural in the PLA/CPO composite after extrusion. Following hot extrusion, the PLA peak is wide and significantly less intense, indicating a less/semi-crystalline phase. The CPO peaks are more visible, confirming that CPO is still present. CPO particles are observed as bright areas dispersed within the PLA

matrix; see Figure 6b. The image shows relatively small CPO particles with a more uniform distribution, though some CPO particles tend to agglomerate in certain areas.

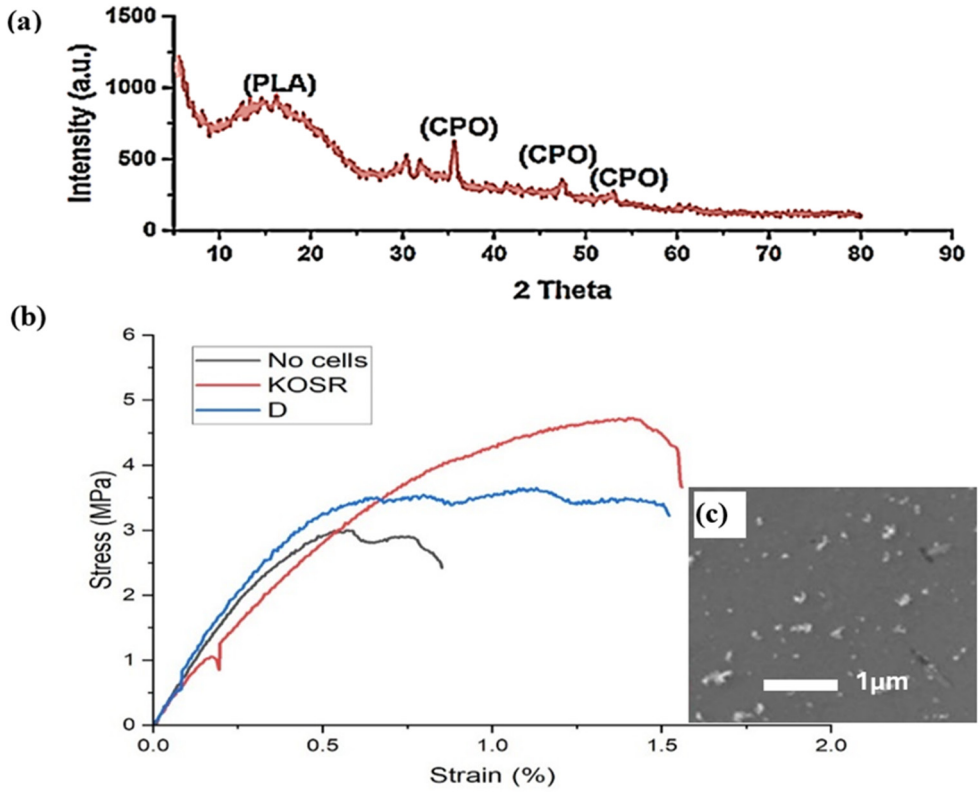



**Figure 6.** (**a**) X-ray diffraction (XRD) of PLA/CPO before and after extrusion, (**b**) Stress strain diagram of filaments containing no cells (gray), with KOSR (blue) and with vitamin D, (**c**) SEM image shows white areas corresponding to CPO particles and grey areas representing the PLA matrix.

The stress–strain diagram in Figure 6b provides a comparison of the mechanical behavior of PLA/CPO composite filaments under different conditions: No Cells (black line), KOSR (red line), and D (vitamin D-blue line). The figure shows how osteogenic differentiation influences filaments' mechanical properties. The No Cells control filament, which was left in solution for 2 weeks without cell integration, exhibits the lowest mechanical performance, with a tensile strength of approximately 2.8 MPa and a strain of ~0.7%. The early failure and limited ductility indicate that PLA/CPO degradation weakened the filament's structure. On the other hand, PLA/CPO cultured with KOSR and D differentiation media exhibit a significant increase in both tensile strength and strain, confirming the reinforcing effect of cell integration. The KOSR filaments demonstrate the highest mechanical improvement, with a tensile strength of ~5 MPa and a strain of ~1.6%, outperforming both the D and the No Cells samples. The almost twofold increase in strength and strain for both cell-cultured filaments highlights the role of osteogenic differentiation in improving the samples' flexibility and structural resilience. These improvements are likely attributed to early extracellular matrix (ECM) deposition by differentiating cells. As cells adhere to the scaffold and begin to remodel their microenvironment, secreted collagen and other matrix proteins form a cohesive interface that enhances the mechanical integrity. Such biological reinforcement is characteristic of early-stage osteogenesis and reflects the scaffold's potential to support functional tissue development.

A key observation is that the KOSR filaments maintain strength over a larger strain range before ultimate failure. This behavior indicates that osteogenic cells within the KOSR environment have a greater capacity to enhance filaments' mechanical properties, likely due to ECM deposition and stronger cell–matrix interactions. The D filaments also show

improved mechanical performance compared to the No Cells control, but its strength and strain values remain lower than KOSR. Another important distinction is the mode of failure across the filaments. The No Cells filaments exhibit brittle failure, failing at lower stress and strain levels, whereas both KOSR and D filaments show improved toughness and resistance to early failure. This suggests that cellular remodeling not only enhances the load-bearing capacity but also improves ductility and energy dissipation prior to fracture. This behavior confirms that biological integration reinforces the filament's structure, delaying the onset of failure and allowing greater energy absorption before breaking. These results indicate that PLA/CPO decomposition over time contributes to mechanical degradation. However, cell integration significantly strengthens the material, with KOSR treatment yielding the most pronounced mechanical enhancement.

## 4. Conclusions

This study enhances bone tissue engineering by introducing a PLA/CPO composite scaffold fabricated via FDM. The oxygen release of the filaments exhibited a gradual increase over 3 days, confirming that CPO hydrolysis occurs as the material absorbs fluid. This early oxygenation may support osteogenic activity and cell viability in vitro, which are essential for bone tissue formation. The research highlights that optimal scaffold quality and accuracy are achieved at a printing speed of 75 mm/s. The PLA/CPO scaffold, featuring 25% porosity and 0.60 mm pore size, showed enhanced expression of osteogenic markers, especially when supplemented with osteogenic media, leading to marked upregulation of the RUNX2 gene which induces the upregulation of SPP1 and SP7, leading to increased proliferation and differentiation towards osteobalst –lineage. Due to upregulation of RUNX2, SPP1 and SP7 and relative downregulation of COL1a1 would be indicative of early Osteoblast-lineage differentiation. Mechanical testing revealed improved properties after cell culturing, with notable increases in tensile strength (approximately 2 MPa) and strain (around 0.7%). These results suggest that the PLA/CPO scaffold supports effective bone regeneration highlighting its potential for further investigation as a scaffold system in bone tissue engineering.

**Author Contributions:** Conceptualization, A.M. (Adnan Memić), A.T., W.R.W., A.A.M., A.M. (Abdullah Mohammed), M.A., A.E., H.H. and K.E.; methodology, A.M. (Adnan Memić), A.T., W.R.W. and M.A.; software, A.M. (Abdullah Mohammed), A.T., W.R.W. and M.A.; validation, A.M. (Abdullah Mohammed), A.T., W.R.W., A.M. (Adnan Memić), M.A. and H.H.; formal analysis, A.M. (Adnan Memić), A.T., W.R.W., A.A.M., A.M. (Abdullah Mohammed), M.A., A.E., H.H. and K.E; investigation, A.M. (Abdullah Mohammed), A.T., W.R.W. and M.A.; resources, A.T., W.R.W., A.A.M., A.M. (Adnan Memić), A.E., H.H. and K.E.; data curation, A.M. (Abdullah Mohammed), A.T., W.R.W. and M.A.; writing—original draft preparation, A.M. (Abdullah Mohammed), A.T., W.R.W., M.A. and H.H.; writing—review and editing, A.M. (Adnan Memić), A.T., W.R.W., A.A.M., A.M. (Abdullah Mohammed), M.A., A.E., H.H. and K.E.; visualization, A.M. (Abdullah Mohammed), A.T., W.R.W., M.A. and H.H.; supervision, W.R.W., A.A.M., A.M. (Adnan Memić), A.E., H.H. and K.E.; project administration, W.R.W., A.A.M., A.M. (Adnan Memić), A.E., H.H. and K.E.; funding acquisition, W.R.W., A.A.M., A.M. (Adnan Memić), A.E., H.H. and K.E. All authors have read and agreed to the published version of the manuscript.

**Funding:** Deanship of Scientific Research (DSR) at King Abdulaziz University, Jeddah: GPIP:1846-903-2024.

**Data Availability Statement:** The data supporting the conclusions of this article will be made available by the authors on request.

**Acknowledgments:** This project was funded by the Deanship of Scientific Research (DSR) at King Abdulaziz University, Jeddah, under grant no. (GPIP:1846-903-2024). The authors, therefore, acknowledge with thanks DSR for technical and financial support.

**Conflicts of Interest:** The authors declare no conflict of interest.

## References

1. United States Department of Health And Human Services. Organ Donation Statistics. Available online: https://www.organdonor.gov/learn/organ-donation-statistics (accessed on 30 April 2025).
2. Centers for Disease Control and Prevention (CDC). Key Facts About Organ Transplant Safety. Available online: https://www.cdc.gov/transplantsafety/overview/key-facts.html (accessed on 15 September 2024).
3. Kumar, P.; Vinitha, B.; Fathima, G. Bone grafts in dentistry. *J. Pharm. Bioallied Sci.* **2013**, *5*, S125–S127. [CrossRef]
4. Brydone, A.S.; Meek, D.; Maclaine, S. Bone grafting, orthopaedic biomaterials, and the clinical need for bone engineering. *Proc. Inst. Mech. Eng. Part H J. Eng. Med.* **2010**, *224*, 1329–1343. (In English) [CrossRef] [PubMed]
5. Dimitriou, R.; Jones, E.; McGonagle, D.; Giannoudis, P.V. Bone regeneration: Current concepts and future directions. *BMC Med.* **2011**, *9*, 66. (In English) [CrossRef]
6. Barua, S.; Chattopadhyay, P.; Aidew, L.; Buragohain, A.K.; Karak, N. Infection-resistant hyperbranched epoxy nanocomposite as a scaffold for skin tissue regeneration. *Polym. Int.* **2015**, *64*, 303–311. [CrossRef]
7. Suvarnapathaki, S.; Wu, X.; Lantigua, D.; Nguyen, M.A.; Camci-Unal, G. Breathing life into engineered tissues using oxygen-releasing biomaterials. *NPG Asia Mater.* **2019**, *11*, 65. [CrossRef]
8. Xiao, Y.; Ahadian, S.; Radisic, M. Biochemical and Biophysical Cues in Matrix Design for Chronic and Diabetic Wound Treatment. *Tissue Eng. Part B Rev.* **2017**, *23*, 9–26. (In English) [CrossRef]
9. Bose, S.; Ke, D.; Sahasrabudhe, H.; Bandyopadhyay, A. Additive manufacturing of biomaterials. *Prog. Mater. Sci.* **2018**, *93*, 45–111. (In English) [CrossRef]
10. Mohammed, A.; Jiménez, A.; Bidare, P.; Elshaer, A.; Memic, A.; Hassanin, H.; Essa, K. Review on Engineering of Bone Scaffolds Using Conventional and Additive Manufacturing Technologies. *3D Print. Addit. Manuf.* **2024**, *11*, 1418–1440. [CrossRef]
11. Ferrari, A.; Baumann, M.; Coenen, C.; Frank, D.; Hennen, L.; Moniz, A.; Torgersen, H.; Torgersen, J.; van Bodegom, L.; van Duijne, F.; et al. *Additive Bio-Manufacturing: 3D Printing for Medical Recovery and Human Enhancement*; European Parliament: Strasbourg, France, 2018.
12. Felfel, R.M.; Poocza, L.; Gimeno-Fabra, M.; Milde, T.; Hildebrand, G.; Ahmed, I.; Scotchford, C.; Sottile, V.; Grant, D.M.; Liefeith, K. In vitro degradation and mechanical properties of PLA-PCL copolymer unit cell scaffolds generated by two-photon polymerization. *Biomed. Mater.* **2016**, *11*, 015011. [CrossRef]
13. Chia, H.N.; Wu, B.M. Recent advances in 3D printing of biomaterials. *J. Biol. Eng.* **2015**, *9*, 4. [CrossRef]
14. Raeisdasteh Hokmabad, V.; Davaran, S.; Ramazani, A.; Salehi, R. Design and fabrication of porous biodegradable scaffolds: A strategy for tissue engineering. *J. Biomater. Sci. Polym. Ed.* **2017**, *28*, 1797–1825. [CrossRef] [PubMed]
15. Armentano, I.; Bitinis, N.; Fortunati, E.; Mattioli, S.; Rescignano, N.; Verdejo, R.; Lopez-Manchado, M.; Kenny, J. Multifunctional nanostructured PLA materials for packaging and tissue engineering. *Prog. Polym. Sci.* **2013**, *38*, 1720–1747. [CrossRef]
16. Lasprilla, A.J.R.; Martinez, G.A.R.; Lunelli, B.H.; Jardini, A.L.; Filho, R.M. Poly-lactic acid synthesis for application in biomedical devices—A review. *Biotechnol. Adv.* **2012**, *30*, 321–328. [CrossRef]
17. Tyler, B.; Gullotti, D.; Mangraviti, A.; Utsuki, T.; Brem, H. Polylactic acid (PLA) controlled delivery carriers for biomedical applications. *Adv. Drug Deliv. Rev.* **2016**, *107*, 163–175. [CrossRef]
18. Gholipourmalekabadi, M.; Zhao, S.; Harrison, B.S.; Mozafari, M.; Seifalian, A.M. Oxygen-Generating Biomaterials: A New, Viable Paradigm for Tissue Engineering? *Trends Biotechnol.* **2016**, *34*, 1010–1021. [CrossRef]
19. Oh, S.H.; Ward, C.L.; Atala, A.; Yoo, J.J.; Harrison, B.S. Oxygen generating scaffolds for enhancing engineered tissue survival. *Biomaterials* **2009**, *30*, 757–762. [CrossRef] [PubMed]
20. Camci-Unal, G.; Alemdar, N.; Annabi, N.; Khademhosseini, A. Oxygen Releasing Biomaterials for Tissue Engineering. *Polym. Int.* **2013**, *62*, 843–848. (In English) [CrossRef]
21. Pedraza, E.; Coronel, M.M.; Fraker, C.A.; Ricordi, C.; Stabler, C.L. Preventing hypoxia-induced cell death in beta cells and islets via hydrolytically activated, oxygen-generating biomaterials. *Proc. Natl. Acad. Sci. USA* **2012**, *109*, 4245–4250. (In English) [CrossRef]
22. Cassidy, D.P.; Irvine, R.L. Use of calcium peroxide to provide oxygen for contaminant biodegradation in a saturated soil. *J. Hazard. Mater.* **1999**, *69*, 25–39. [CrossRef]
23. Waite, A.J.; Bonner, J.S.; Autenrieth, R. Kinetics and Stoichiometry of Oxygen Release from Solid Peroxides. *Environ. Eng. Sci.* **1999**, *16*, 187–199. [CrossRef]
24. Mohammed, A.H.; Kovacev, N.; Elshaer, A.; Melaibari, A.A.; Iqbal, J.; Hassanin, H.; Memić, A. Preparation of Polylactic Acid/Calcium Peroxide Composite Filaments for Fused Deposition Modelling. *Polymers* **2023**, *15*, 2229. [CrossRef] [PubMed]

25. Mohammed, A.; Saeed, A.; Elshaer, A.; Melaibari, A.A.; Memić, A.; Hassanin, H.; Essa, K. Fabrication and Characterization of Oxygen-Generating Polylactic Acid/Calcium Peroxide Composite Filaments for Bone Scaffolds. *Pharmaceuticals* **2023**, *16*, 627. [CrossRef]
26. Mota, C.; Puppi, D.; Chiellini, F.; Chiellini, E. Additive manufacturing techniques for the production of tissue engineering constructs. *J. Tissue Eng. Regen. Med.* **2015**, *9*, 174–190. [CrossRef]
27. Li, C.; Zhang, J.; Han, J.; Yao, B. A numerical solution to the effects of surface roughness on water–coal contact angle. *Sci. Rep.* **2021**, *11*, 459. [CrossRef]
28. Yu, W.; Shi, J.; Sun, L.; Lei, W. Effects of Printing Parameters on Properties of FDM 3D Printed Residue of Astragalus/Polylactic Acid Biomass Composites. *Molecules* **2022**, *27*, 7373. [CrossRef] [PubMed]
29. Lee, J.Y.; Kwon, S.H.; Chin, I.-J.; Choi, H.J. Toughness and rheological characteristics of poly(lactic acid)/acrylic core–shell rubber blends. *Polym. Bull.* **2019**, *76*, 5483–5497. [CrossRef]
30. Breeland, G.; Sinkler, M.A.; Menezes, R.G. Embryology, bone ossification. In *StatPearls [Internet]*; StatPearls Publishing: Treasure Island, FL, USA, 2021.
31. Feng, X. Chemical and Biochemical Basis of Cell-Bone Matrix Interaction in Health and Disease. *Curr. Chem. Biol.* **2009**, *3*, 189–196. (In English) [CrossRef] [PubMed]
32. Boraschi-Diaz, I.; Wang, J.; Mort, J.S.; Komarova, S.V. Collagen Type I as a Ligand for Receptor-Mediated Signaling. *Front. Phys.* **2017**, *5*, 12. (In English) [CrossRef]
33. Komori, T. Regulation of osteoblast differentiation by Runx2. *Adv. Exp. Med. Biol.* **2010**, *658*, 43–49. (In English) [CrossRef]
34. Choi, J.U.A.; Kijas, A.W.; Lauko, J.; Rowan, A.E. The Mechanosensory Role of Osteocytes and Implications for Bone Health and Disease States. *Front. Cell Dev. Biol.* **2022**, *9*, 770143. (In English) [CrossRef]
35. Liu, Q.; Li, M.; Wang, S.; Xiao, Z.; Xiong, Y.; Wang, G. Recent Advances of Osterix Transcription Factor in Osteoblast Differentiation and Bone Formation. *Front. Cell Dev. Biol.* **2020**, *8*, 601224. (In English) [CrossRef] [PubMed]
36. De Luca, A.; Vitrano, I.; Costa, V.; Raimondi, L.; Carina, V.; Bellavia, D.; Conoscenti, G.; Di Falco, R.; Pavia, F.C.; La Carrubba, V.; et al. Improvement of osteogenic differentiation of human mesenchymal stem cells on composite poly l-lactic acid/nano-hydroxyapatite scaffolds for bone defect repair. *J. Biosci. Bioeng.* **2019**, *129*, 250–257. [CrossRef] [PubMed]


**Disclaimer/Publisher's Note:** The statements, opinions and data contained in all publications are solely those of the individual author(s) and contributor(s) and not of MDPI and/or the editor(s). MDPI and/or the editor(s) disclaim responsibility for any injury to people or property resulting from any ideas, methods, instructions or products referred to in the content.